Nigerian Journal of Physics (NJP)
ISSN online: 3027-0936
ISSN print: 1595-0611
DOI: https://doi.org/10.62292/njp.v33(s).2024.258
Volume 33(S) 2024

# Fractional Derivative Models for Energy Levels and Molar Entropy of Diatomic Molecules

***[1]Ahmed, A. D., [1]Eyube, E. S., [2]Mohammed, B. D., [3]Ayuba, J. B. and [4]Sabo, B.**

[1]Department of Physics, Faculty of Physical Sciences, Modibbo Adama University, P.M.B. 2076, Yola, Adamawa State, Nigeria.
[2]Department of Science Laboratory Technology, School of Science and Technology, Adamawa State Polytechnic, P.M.B. 2146, Yola, Adamawa State, Nigeria.
[3]Department of Science Laboratory Technology, Adamawa State College of Agriculture, Ganye, Nigeria
[4]Department of Physics, Aminu Saleh College of Education, Azare, Nigeria

[*]Corresponding author's email: adahmed19@mau.edu.ng Phone: +2348065326308

**ABSTRACT**
This study develops new analytical equations for the energy levels and molar entropy of substances by solving the Schrödinger equation with the Pöschl-Teller potential. While thermodynamics is crucial in fields like agriculture, drug design, and medical research, existing models often use spectroscopic constants but overlook fractional parameters, which limits their accuracy for gaseous diatomic molecules. By integrating fractional parameters alongside spectroscopic constants, this study addresses this limitation and improves precision. The new equations are applied to analyze pure substances, including $Br_2$ ($X\ ^1\sum_g^+$), $Cl_2$ ($X\ ^1\sum_g^+$), CO ($X\ ^1\sum^+$), and $Na_2$ ($X\ ^1\sum_g^+$). The mean percentage absolute deviation (MPAD) of the energy levels obtained is 1.4797%, 0.9043%, 0.0898%, and 1.1352%, respectively, compared to Rydberg-Klein-Rees data. For molar entropy, the MPAD values are 0.1381%, 0.1360%, 0.1322%, and 0.6437% relative to data from the National Institute of Standards and Technology (NIST) database. These results indicate a significant improvement in accuracy over existing models and are consistent with the literature on gaseous molecules.

**Keywords:**
Diatomic molecules,
Fractional parameters,
Thermodynamic functions,
Energy eigenvalues.

## INTRODUCTION

Thermodynamics is a highly useful field in the physical sciences that has significantly influenced human livelihood. Studies in thermodynamics have been crucial for investigating the growth reactions of economically important plants in agriculture (Popovic and Minceva, 2021). Thermodynamic measurements have played a pivotal role in the efficient design and manufacture of drugs in the chemical industry (Garbett and Chaires2012). Moreover, thermodynamic processes have been applied in medical research to diagnose, evaluate, and treat certain ailments such as cancer (Shamsabadipour et al., 2023). Furthermore, thermodynamics has been instrumental in selecting phases during the non-equilibrium processing of materials.

Determining the thermal properties of real substances involves measuring various physical quantities, such as energy, entropy, heat capacity, and enthalpy. For example, William et al. experimentally determined the configurational entropy in a two-dimensional liquid subjected to random spinning (Williams et al., 2018). Given the high costs and complexity of these experimental setups, scientists have developed analytical models to analyze the thermal properties of substances. These models have proven essential in predicting the thermodynamic properties of various substances (Strekalov, 2024).

A key feature of these models is the type of diatomic molecule oscillator used to define the vibrational energy levels of the system. In a recent study, thermodynamic model equations derived from the shifted Morse potential have been essential for investigating the molar entropy, enthalpy, Gibbs free energy, and heat capacity of nitrogen and iodine dimers (Onate et al, 2024). Additionally, model equations based on the deformed Pöschl-Teller oscillator have been developed to predict the thermochemical properties of various substances. These equations have been applied to estimate the thermal properties of gaseous molecules such as $P_2$, $N_2$, and ICl (Eyube et al., 2022).

The improved Generalized Pöschl-Teller (IGPT) oscillator is widely recognized for its accuracy to replicating experimental potential energy data in numerous diatomic molecules. Its equation for energy levels has successfully contributed to formulating thermodynamic models for gaseous molecules. Ro-vibrational energy levels of diatomic molecules have been derived by solving the Schrödinger equation with and without electromagnetic potential coupling under the IGPT oscillator (Yanar et al., 2020). Analytical equations predicting Gibbs free energy and heat capacity of gaseous molecules have been obtained using the energy levels equation of the IGPT potential. These equations were applied to predict the thermal properties of ground state $Br_2$, $Cl_2$, and CO molecules (Eyube, Onate, Omugbe and Nwabueze 2022). The equation describing the internal motion of the IGPT oscillator is given as (Yanar et al., 2020)

$$U(\rho) = D_e\left\{1 + \frac{1+cosh^2(\alpha\rho_e)-2\,cosh(\alpha\rho_e)\,cosh(\alpha\rho)}{sinh^2(\alpha\rho)}\right\},$$
$$\alpha = \pi c\omega_e\left(\frac{2\mu}{D_e}\right)^{\frac{1}{2}}, \qquad (1)$$

where $D_e$, $\rho_e$, and $\alpha$ are the equilibrium dissociation energy, bond length, and potential screening parameter, respectively. $\omega_e$ stands for the equilibrium harmonic vibrational frequency, $c$ signifies the speed of light, $\rho$ is the internuclear distance and $\mu$ indicates the reduced mass of a diatomic molecule.

Fractional calculus has gained significant attention from researchers in recent years, drawing interest across various scientific and technological disciplines. It involves differentiating and integrating non-integer orders, which differs from traditional integer-order calculus. Recent advancements in fractional calculus include various formulations and methodologies, such as the generalized fractional derivative approach discussed in recent literature (Abu-Shady, Khokha and Abdel-Karim, 2022). This method aids in deriving more precise expressions for bound-state energy levels in potential systems such as the improved Tietz potential (Abu-Shady, Khokha, 2022). The enhanced accuracy of these models stems from the incorporation of fractional parameters within the equations (Abu-Shady and Khokha, 2023).

Despite significant advancements in predicting the energy spectra of diatomic molecules, thermodynamic models often overlook fractional parameters. This omission can undermine the accuracy of predictions for thermal properties in gaseous molecules. To address this issue, our study develops new equations that incorporate fractional parameters for both energy levels and molar entropy of diatomic molecules, extending the IGPT potential model. This approach aims to enhance the precision and reliability of thermal property predictions, including those related to energy levels.

## Fractional energy levels and molar entropy model of the IGPT potential

### *An overview of the GFNU method*

The fractional derivative is a mathematical operation that involves differentiation of fractional orders, distinguishing it from the standard integer-order calculus operations. Fractional derivative finds application across various fields of science and technology. Different definitions of fractional calculus, such as those by Jumarie, Riemann-Liouville, Caputo, and the generalized fractional derivative (GFD) method have been formulated to suit different applications, particularly in physics (Abu-Shady, Fath-Allah, 2023). Based on the GFD approach, the derivative of a function $\psi(\tau)$ is given as

$$\Delta\psi(\tau) = \lim_{q\to 0}\frac{\psi(\tau+q\tau^{1-p})-\psi(\tau)}{q}, \qquad (2)$$

where $q = \frac{\Gamma(Q)}{\Gamma(Q-p+1)}$, $\Delta$ is a generalized fractional differential operator. $p$ and $Q$ are fractional parameters satisfying $0 < p \leq 1$, $Q \in R^+$, and $\Gamma(x)$ denotes the standard gamma function evaluated at $x$. The operator $\Delta$ has the property that

$$\Delta^p\{\psi(\tau)\} = q\tau^{1-p}\psi'(\tau)$$
$$\Delta^p\{\Delta^p\psi(\tau)\} = q^2\{\tau^{1-p}\psi''(\tau) + (1-p)\tau^{1-2p}\psi'(\tau)\}. \qquad (3)$$

Recently, the parametric GFNU was introduced to solve Schrödinger and other wave equations. By suitably transforming the Schrödinger equation to the form (Abu-Shady, Fath-Allah, 2023)

$$\Delta^p\left[\Delta^p u_{npq}(s)\right] + \frac{\alpha_1-\alpha_2 s}{s(1-\alpha_3 s)}\Delta^p u_{npq}(s) + \frac{-\xi_1 s^{2p}+\xi_2 s^p-\xi_3}{s^{2p}(1-\alpha_3 s^p)^2}u_{npq}(s) = 0, \qquad (4)$$

in which $u_{npq}(s)$ is the wave function $n$ denotes the vibrational quantum number $n$ = 0, 1, 2, …. The condition leading to bound state solutions is given as (Abu-Shady, Fath-Allah, 2023)

$$n^2\alpha_3 p^2q^2 + n(\alpha_2-\alpha_3 pq)pq - (2n+1)\alpha_5 pq + (2n+1)\left(\sqrt{\alpha_9}+\alpha_3\sqrt{\alpha_8}\right)pq + \alpha_7 + 2\alpha_3\alpha_8 + 2\sqrt{\alpha_8\alpha_9} = 0, \qquad (5)$$

where

$$\alpha_4 = \frac{1}{2}(pq-\alpha_1), \quad \alpha_5 = \frac{1}{2}(\alpha_2 - 2\alpha_3 pq)$$
$$\alpha_6 = \alpha_5^2 + \xi_1, \quad \alpha_7 = 2\alpha_4\alpha_5 - \xi_2, \alpha_8 = \alpha_4^2 + \xi_3$$
$$\alpha_9 = \alpha_3\alpha_7 + \alpha_3^2\alpha_8 + \alpha_6. \qquad (6)$$

Equations (4) and (5) provide the framework for developing the expression for the energy spectrum and consequently the generalized internal partition function for gaseous molecules.

***Ro-vibrational energy states of the IGPT oscillator***

The radial Schrödinger equation for the IGPT potential is written as

$$u''_{npQ}(\rho)+\frac{2M}{\hbar^2}\left\{E_{npQ}-D_e-\frac{U_1-U_2\,cosh(\alpha\rho)}{sinh^2(\alpha\rho)}\right\}u_{npQ}(\rho)=0, \quad (7)$$

here, $M$ and $\hbar$ represent the reduced mass and reduced Planck constant, respectively. Equation (7) is transformed into a hypergeometric equation using the substitution $s = \tanh^2(½\alpha\rho)$ to obtain

$$u''_{npQ}(s)+\frac{\frac{1}{2}(1-3s)}{s(1-s)}u'_{npQ}(s)+\frac{-\varepsilon_1 s^2+\varepsilon_2 s-\varepsilon_3}{s^2(1-s)^2}u_{npQ}(s)=0. \quad (8)$$

where

$$\varepsilon_1=\frac{2MD_e\,cosh^4\left(\frac{1}{2}\alpha\rho_e\right)}{\alpha^2\hbar^2},\ \varepsilon_2=\frac{2M}{\alpha^2\hbar^2}\left[E_{npQ}+\frac{1}{2}D_e\,sinh^2(\alpha\rho_e)\right],\ \varepsilon_3=\frac{2MD_e\,sinh^4\left(\frac{1}{2}\alpha\rho_e\right)}{\alpha^2\hbar^2}. \quad (9)$$

Equation (8) can typically be solved using standard methods for hypergeometric differential equations. However, a more precise determination of energy eigenvalues can be achieved using a fractional calculus approach. The equivalent GFD form of this equation is obtained by replacing integer orders with fractional parameters (Abu-Shady, Fath-Allah, 2023), resulting in

$$\Delta^p\left[\Delta^p u_{npQ}(s)\right]+\frac{\frac{1}{2}(1-3s^p)}{s^p(1-s^p)}\Delta^p u_{npQ}(s)+\frac{-\varepsilon_1 s^{2p}+\varepsilon_2 s^p-\varepsilon_3}{s^{2p}(1-s^p)^2}u_{npQ}(s)=0. \quad (10)$$

Equations (10) and (4) are the same if $\alpha_1=\frac{1}{2}$, $\alpha_2=\frac{3}{2}$, $\alpha_3=1$, $\xi_1=\varepsilon_1$, $\xi_2=\varepsilon_2$, $\xi_3=\varepsilon_3$. These values substituted into (6) gives $\alpha_4=\frac{1}{2}pq-\frac{1}{4}$, $\alpha_5=-pq+\frac{3}{4}$, $\alpha_6=\left(pq-\frac{3}{4}\right)^2+\varepsilon_1$, $\alpha_7=-\left(pq-\frac{1}{2}\right)\left(pq-\frac{3}{4}\right)-\varepsilon_2$, $\alpha_8=\frac{1}{4}\left(pq-\frac{1}{2}\right)^2+\varepsilon_3$, and $\alpha_9=\frac{1}{4}(pq-1)^2+\varepsilon_1-\varepsilon_2+\varepsilon_3$. Using these results in (5), we derive

$$\varepsilon_2=\varepsilon_1+\varepsilon_3+\frac{1}{4}(pq-1)^2-p^2q^2\times\left\{n+\frac{1}{2}-\sqrt{\left(\frac{1}{2}-\frac{3}{4pq}\right)^2+\frac{\varepsilon_1}{p^2q^2}}+\sqrt{\left(\frac{1}{2}-\frac{1}{4pq}\right)^2+\frac{\varepsilon_3}{p^2q^2}}\right\}^2. \quad (11)$$

Combining equations (11) and (9), we have the fractional energy eigenvalue equation for the pure vibrational state of the IGPT oscillator as follows

$$E_{npQ}=D_e+\frac{\alpha^2\hbar^2}{8M}(pq-1)^2-\frac{\alpha^2\hbar^2}{2M}p^2q^2\times\left\{n+\frac{1}{2}-\sqrt{\left(\frac{1}{2}-\frac{3}{4pq}\right)^2+\frac{2MD_e\,cosh^4\left(\frac{1}{2}\alpha\rho_e\right)}{\alpha^2\hbar^2p^2q^2}}+\sqrt{\left(\frac{1}{2}-\frac{1}{4pq}\right)^2+\frac{2MD_e\,sinh^4\left(\frac{1}{2}\alpha\rho_e\right)}{\alpha^2\hbar^2p^2q^2}}\right\}^2. \quad (12)$$

***The internal partition functions***

The internal partition functions are crucial for deriving thermodynamic models applicable to gaseous molecules. At a temperature $T$, the internal partition function of a diatomic system is expressed as $Z = Z_{vib}(T)Z_{rot}(T)Z_{tra}(T)$, where $Z_{vib}$, $Z_{rot}$, and $Z_{tra}$ denote the vibrational, rotational, and translational partition functions, respectively. The temperature dependence of $Z_{vib}$ is detailed in (Ahmed, Eyube, Omugbe, Onate and Timtere, 2023)

$$Z_{vib}=\sum_{n=0}^{\sigma}e^{-\gamma E_{npq}}, \quad (13)$$

here, $\gamma^{-1} = k_BT$, where $k_B$ is the Boltzmann coefficient, and $n_{max}$ represents the number of excited bonded states found by imposing the condition $\left.\frac{\partial E_{npq}}{\partial n}\right|_{\sigma}=0$. Plugging equation (12) into this expression yields

$$\sigma=-\frac{1}{2}+\sqrt{\left(\frac{1}{2}-\frac{3}{4pq}\right)^2+\frac{2MD_e\,cosh^4\left(\frac{1}{2}\alpha\rho_e\right)}{\alpha^2\hbar^2p^2q^2}}-\sqrt{\left(\frac{1}{2}-\frac{1}{4pq}\right)^2+\frac{2MD_e\,sinh^4\left(\frac{1}{2}\alpha\rho_e\right)}{\alpha^2\hbar^2p^2q^2}}. \quad (14)$$

Inserting equations (12) into (13), one obtains

$$Z_{vib}=e^{-\omega^2}\sum_{n=0}^{\sigma}e^{\kappa^2\left(\frac{n}{\sigma}-1\right)^2}, \quad (15)$$

where $\omega=\sqrt{\gamma\left\{D_e+\frac{1}{8}\alpha^2\hbar^2M^{-1}(pq-1)^2\right\}}$, and $\kappa=\alpha\hbar\sigma pq\sqrt{\frac{1}{2}\gamma M^{-1}}$. The exponential function in series (15) precludes exact evaluation. However, the modified Poisson summation approach allows for deriving an approximate expression for the vibrational partition function Eyube, Onate, Omugbe and Nwabueze (2022) outlines this method as follows

$$\sum_{n=0}^{n=\sigma}\xi(n)=\frac{1}{2}\{\xi(0)-\xi(\sigma+1)\}+\int_0^{\sigma+1}\xi(x)dx, \quad (16)$$

Using expression (16) to evaluate summation, equation (15) is rewritten as

$$Z_{vib}=\frac{1}{2}e^{\kappa^2-\omega^2}-\frac{1}{2}e^{\frac{\kappa^2}{\sigma^2}-\omega^2}+\frac{\sigma\sqrt{\pi}}{2\kappa}e^{-\omega^2}\left(\mathrm{erfi}\kappa+\mathrm{erfi}\frac{\kappa}{\sigma}\right), \quad (17)$$

where erfi $x$ is the imaginary error function evaluated at $x$. In the framework of the rigid rotor approximation for a diatomic molecule, the rotational partition function $Z_{rot}$ and the translational partition function $Z_{tra}$ are expressed as (Ahmed, Eyube, Omugbe, Onate and Timtere, 2023).

$$Z_{rot}=\frac{1}{\Omega}\left(\frac{1}{3}+\frac{\tau}{\gamma}+\frac{\gamma}{15\tau}+\frac{4\gamma^2}{315\tau^2}\right), \quad (18)$$

$$Z_{tra}=\frac{1}{P}\left(\frac{M_0}{2\pi\hbar^2}\right)^{\frac{3}{2}}\gamma^{-\frac{5}{2}}, \quad (19)$$

in this context, $\mu_0$ represents the molar mass, $P$ signifies the pressure, and $\tau=\frac{\hbar^2}{2\mu r_e^2}$. The parameter $\Omega$ distinguishes between homonuclear molecules ($\Omega = 2$) and heteronuclear molecules ($\Omega = 1$), reflecting their respective symmetry coefficients. The molar entropy is derived from the expression $S_{pQ}=R\left(ln\,Z-\gamma\frac{\partial}{\partial\gamma}ln\,Z\right)$, where R is the molar gas constant. This expression, in conjunction with equations (17), (18), and (19), is used to derive the fractional equation for the molar entropy of the IGPT oscillator, given by

$$S_{pQ} = R\left\{ ln\,\mathrm{Z} + \omega^2 + \frac{5}{2} - \frac{(\kappa^2+\sigma)\,e^{\kappa^2-\omega^2} - \left(\frac{\kappa^2}{\sigma^2}-1\right) e^{\frac{\kappa^2}{\sigma^2}-\omega^2} - \frac{\sigma\sqrt{\pi}\,\mathrm{erfi}\kappa + \mathrm{erfi}\frac{\kappa}{\sigma}}{2\ \ \kappa e^{\omega^2}}}{2Z_{\mathrm{vib}}} + \frac{\frac{\tau}{\gamma} - \frac{\gamma}{15\tau} - \frac{8\gamma^2}{315\tau^2}}{\Omega Z_{\mathrm{rot}}} \right\}. \quad (20)$$

## RESULTS AND DISCUSSION

Notably, when the fractional parameters are set to $p = Q = 1$, the parameter $q$ also equals 1. Under these conditions, Equation (12) simplifies to

$$E_n = D_e - \frac{\alpha^2\hbar^2}{2M}\left\{ n + \frac{1}{2} - \sqrt{\frac{1}{16} + \frac{2MD_e\,cosh^4\left(\frac{1}{2}\alpha\rho_e\right)}{\alpha^2\hbar^2}} + \sqrt{\frac{1}{16} + \frac{2MD_e\,sinh^4\left(\frac{1}{2}\alpha\rho_e\right)}{\alpha^2\hbar^2}} \right\}^2. \quad (21)$$

Equation (21) represents the pure vibrational state energy spectrum of the IGPT oscillator, as described in the works of Yanar et al. (2020). This indicates that Equation (12) provides the most general form for the pure vibrational energy spectrum of the IGPT potential.

To assess the applicability of this energy level equation to real systems, four diatomic molecules are examined: $Br_2$ ($X\ ^1\sum_g^+$), $Cl_2$ ($X\ ^1\sum_g^+$), CO ($X\ ^1\sum^+$) and $Na_2$ ($X\ ^1\sum_g^+$). These molecules are selected due to their well-documented spectroscopic constants, including equilibrium internuclear distance ($\rho_e$), dissociation energy ($D_e$), and vibrational frequency ($\omega_e$). Experimental data for $D_e$, $\rho_e$, and $\omega_e$ are sourced from Refs. (Focsa et al., 2000; Hajigeorgiou, 2010). Computed values of the screening parameter $\alpha$ for these molecules are also provided in the table.

Using the data from Table 1, Equations (12) and (21) are employed to calculate the eigenenergies of the molecules with and without fractional parameters for various vibrational quantum numbers. Tables 2 and 3 compare these analytically generated energy eigenvalues with the observed energies of $Br_2$ ($X\ ^1\sum_g^+$), $Cl_2$ ($X\ ^1\sum_g^+$), CO ($X\ ^1\sum^+$) and $Na_2$ ($X\ ^1\sum_g^+$) molecules, as reported by the Rydberg-Klein-Rees (RKR) experimental method in Refs. (Kirschner and Watson, 1974; Kusch and Hessel, 1978; Coxon, 1980; Focsa et al., 2000).

**Table 1: Spectroscopic constants and potential screening parameters for diatomic molecules evaluated in this research (Focsa et al., 2000; Hajigeorgiou, 2010)**

| Diatomic molecule | Molecular state | Spectroscopic constant | | | $\alpha$ (Å$^{-1}$) |
|---|---|---|---|---|---|
| | | $\omega_e$ (cm$^{-1}$) | $D_e$ (cm$^{-1}$) | $\rho_e$ (Å) | |
| $Br_2$ | $X\ ^1\sum_g^+$ | 325.314194 | 15894.546 | 2.2810213 | 1.9862 |
| $Cl_2$ | $X\ ^1\sum_g^+$ | 559.7507 | 20276.44 | 1.98720 | 2.0017 |
| CO | $X\ ^1\sum^+$ | 2169.8129 | 90670 | 1.12832320 | 2.2978 |
| $Na_2$ | $X\ ^1\sum_g^+$ | 159.10939 | 5988 | 3.078538 | 0.8489 |

**Table 2: Comparative analysis of pure vibrational state energies (in cm$^{-1}$) relative to experimental RKR energies (in cm$^{-1}$) for diatomic molecules: PAD values as a percentage of RKR energies**

| $n$ | $Br_2$ ($X\ ^1\sum_g^+$) $p$ = 0.9800, $Q$ = 0.4100 | | | | | $n$ | $Cl_2$ ($X\ ^1\sum_g^+$) $p$ = 0.5000, $Q$ = 0.4114 | | | | |
|---|---|---|---|---|---|---|---|---|---|---|---|
| | Eq. (21) | Eq. (12) | [a]$E_{obs}$ | $PAD_1$ | $PAD_2$ | | Eq. (21) | Eq. (12) | [b]$E_{obs}$ | $PAD_1$ | $PAD_2$ |
| 0 | 162.2410 | 166.8772 | 162.3803 | 0.0858 | 2.7694 | 0 | 278.910 | 283.647 | 279.165 | 0.0914 | 1.6056 |
| 1 | 484.2260 | 497.9890 | 485.5306 | 0.2687 | 2.5659 | 1 | 830.934 | 844.948 | 833.463 | 0.3034 | 1.3779 |
| 2 | 802.8820 | 825.5782 | 806.5050 | 0.4492 | 2.3649 | 2 | 1375.233 | 1398.256 | 1382.347 | 0.5146 | 1.1509 |
| 3 | 1118.2089 | 1149.6448 | 1125.2909 | 0.6293 | 2.1642 | 3 | 1911.805 | 1943.572 | 1925.801 | 0.7267 | 0.9228 |
| 4 | 1430.2067 | 1470.1888 | 1441.8750 | 0.8092 | 1.9637 | 4 | 2440.651 | 2480.897 | 2463.794 | 0.9393 | 0.6942 |
| … | … | … | … | … | … | 5 | 2961.771 | 3010.230 | 2996.288 | 1.1520 | 0.4653 |
| 13 | 4088.3766 | 4196.5680 | 4189.6294 | 2.4167 | 0.1656 | 6 | 3475.165 | 3531.571 | 3523.230 | 1.3642 | 0.2367 |
| 14 | 4367.0833 | 4481.8860 | 4483.3568 | 2.5934 | 0.0328 | 7 | 3980.832 | 4044.920 | 4044.564 | 1.5757 | 0.0088 |
| 15 | 4642.4609 | 4763.6815 | 4774.7011 | 2.7696 | 0.2308 | 8 | 4478.773 | 4550.277 | 4560.230 | 1.7862 | 0.2183 |
| 16 | 4914.5094 | 5041.9543 | 5063.6415 | 2.9452 | 0.4283 | 9 | 4968.988 | 5047.642 | 5070.165 | 1.9955 | 0.4442 |
| … | … | … | … | … | … | 10 | 5451.477 | 5537.015 | 5574.305 | 2.2035 | 0.6690 |
| 25 | 7213.1357 | 7387.8929 | 7552.0265 | 4.4874 | 2.1734 | 11 | 5926.239 | 6018.397 | 6072.591 | 2.4100 | 0.8924 |
| 26 | 7451.8930 | 7630.9398 | 7815.5635 | 4.6532 | 2.3623 | 12 | 6393.275 | 6491.786 | 6564.968 | 2.6153 | 1.1147 |
| 27 | 7687.3213 | 7870.4640 | 8076.3966 | 4.8174 | 2.5498 | 13 | 6852.585 | 6957.184 | 7051.387 | 2.8193 | 1.3359 |
| 28 | 7919.4205 | 8106.4657 | 8334.4900 | 4.9801 | 2.7359 | 14 | 7304.169 | 7414.590 | 7531.811 | 3.0224 | 1.5563 |
| 29 | 8148.1905 | 8338.9448 | 8589.8067 | 5.1412 | 2.9205 | 15 | 7748.026 | 7864.004 | 8006.214 | 3.2248 | 1.7762 |
| MPAD (%) | | | | 2.6586 | 1.4797 | MPAD (%) | | | | 1.6715 | 0.9043 |

a: (Focsa et al., 2000); b: (Coxon, 1980)

**Table 3: Comparative analysis of pure vibrational state energies (in cm⁻¹) relative to experimental RKR energies (in cm⁻¹) for diatomic molecules: PAD values as a percentage of RKR energies**

| *n* | CO ($X\ ^1\Sigma^+$) $p$ = 0.9000, $Q$ = 0.7159 | | | | | *n* | $Na_2$ ($X\ ^1\Sigma_g^+$) $p$ = 0.5000, $Q$ = 0.4310 | | | | |
|---|---|---|---|---|---|---|---|---|---|---|---|
| | **Eq. (21)** | **Eq. (12)** | **[c] $E_{obs}$** | **$PAD_1$** | **$PAD_2$** | | **Eq. (21)** | **Eq. (12)** | **[d] $E_{obs}$** | **$PAD_1$** | **$PAD_2$** |
| 0 | 1081.6615 | 1081.0777 | 1081.7791 | 0.0109 | 0.0648 | 0 | 79.290 | 78.004 | 76.391 | 3.7956 | 2.1116 |
| 1 | 3225.5116 | 3223.7815 | 3225.0522 | 0.0142 | 0.0394 | 1 | 236.286 | 232.478 | 228.216 | 3.5361 | 1.8676 |
| 2 | 5343.3990 | 5340.5505 | 5341.8437 | 0.0291 | 0.0242 | 2 | 391.168 | 384.907 | 378.693 | 3.2941 | 1.6408 |
| 3 | 7435.3236 | 7431.3849 | 7432.2200 | 0.0418 | 0.0112 | 3 | 543.935 | 535.290 | 527.810 | 3.0552 | 1.4171 |
| 4 | 9501.2854 | 9496.2847 | 9496.2494 | 0.0530 | 0.0004 | 4 | 694.589 | 683.627 | 675.557 | 2.8173 | 1.1945 |
| … | … | … | … | … | … | 5 | 843.129 | 829.918 | 821.924 | 2.5800 | 0.9727 |
| 15 | 30513.3230 | 30498.4938 | 30482.6901 | 0.1005 | 0.0518 | 6 | 989.555 | 974.164 | 966.898 | 2.3433 | 0.7515 |
| 16 | 32267.7316 | 32252.1776 | 32235.4197 | 0.1002 | 0.0520 | 7 | 1133.868 | 1116.365 | 1110.466 | 2.1074 | 0.5312 |
| 17 | 33996.1775 | 33979.9266 | 33964.8189 | 0.0923 | 0.0445 | 8 | 1276.066 | 1256.520 | 1252.614 | 1.8722 | 0.3118 |
| 18 | 35698.6606 | 35681.7410 | 35667.9725 | 0.0860 | 0.0386 | 9 | 1416.151 | 1394.629 | 1393.327 | 1.6381 | 0.0934 |
| … | … | … | … | … | … | 10 | 1554.121 | 1530.692 | 1532.590 | 1.4049 | 0.1238 |
| 20 | 39025.7385 | 39007.5658 | 38998.8817 | 0.0689 | 0.0223 | 11 | 1689.978 | 1664.710 | 1670.385 | 1.1730 | 0.3397 |
| 21 | 40650.3333 | 40631.5762 | 40626.8057 | 0.0579 | 0.0117 | 12 | 1823.721 | 1796.682 | 1806.696 | 0.9423 | 0.5543 |
| 22 | 42248.9654 | 42229.6520 | 42229.8199 | 0.0453 | 0.0004 | 13 | 1955.350 | 1926.609 | 1941.503 | 0.7132 | 0.7671 |
| 23 | 43821.6346 | 43801.7930 | 43808.0060 | 0.0311 | 0.0142 | 14 | 2084.865 | 2054.490 | 2074.787 | 0.4857 | 0.9783 |
| … | … | … | … | … | … | 15 | 2212.266 | 2180.325 | 2206.527 | 0.2601 | 1.1875 |
| 33 | 58120.3752 | 58096.7970 | 58240.4388 | 0.2062 | 0.2466 | 16 | 2337.553 | 2304.115 | 2336.702 | 0.0364 | 1.3946 |
| 34 | 59407.4541 | 59383.6567 | 59550.0742 | 0.2395 | 0.2795 | 17 | 2460.727 | 2425.859 | 2465.290 | 0.1851 | 1.5994 |
| 35 | 60668.5701 | 60644.5818 | 60835.5899 | 0.2745 | 0.3140 | 18 | 2581.786 | 2545.557 | 2592.266 | 0.4043 | 1.8018 |
| 36 | 61903.7235 | 61879.5721 | 62097.0060 | 0.3113 | 0.3502 | 19 | 2700.732 | 2663.210 | 2717.606 | 0.6209 | 2.0016 |
| 37 | 63112.9140 | 63088.6279 | 63334.3337 | 0.3496 | 0.3880 | 20 | 2817.564 | 2778.817 | 2841.283 | 0.8348 | 2.1985 |
| | | MPAD (%) | | 0.0992 | 0.0898 | | | MPAD (%) | | 1.6238 | 1.1352 |

c: (Kirschner and Watson, 1974); d: (Kusch and Hessel, 1978)

To validate the accuracy of the model equations, the Lippincott error rate standard is utilized. This standard calculates the percentage absolute deviation (PAD) of the calculated results from the observed data, assessing the effectiveness of the model equations. According to the Lippincott standard, a model is deemed satisfactory if the PAD does not exceed 1% of the experimental data; thus, a lower PAD value indicates a better model. The PAD is written as (Eyube et al., 2023)

$$\mathrm{PAD} = 100\left|\frac{A-B}{C}\right|_n, \qquad (22)$$

where $A$, $B$, and $C$ are parameters to be chosen, with $A = C = E_{obs}$ and $B = (E_n, E_{npQ})$ [front]. The percentage absolute deviations (PADs), denoted as $PAD_1$ for the model without fractional parameters and $PAD_2$ for the model with fractional parameters, are calculated for the molecules and listed in Tables 2 and 3.

The results clearly show that the PAD values computed using equations with fractional parameters are lower compared to those computed without fractional parameters. This suggests that incorporating fractional parameters into the energy spectrum model significantly enhances its accuracy. The mean percentage absolute deviation ($\mathrm{MPAD} = \frac{1}{N_p}\sum_{j=1}^{N_p}\mathrm{PAD}_j$) values, where $N_p$ represents the number of RKR data points, are calculated to illustrate the impact of fractional parameters. For the $Br_2$ ($X\ ^1\Sigma_g^+$), $Cl_2$ ($X\ ^1\Sigma_g^+$), CO ($X\ ^1\Sigma^+$) and $Na_2$ ($X\ ^1\Sigma_g^+$) molecules, the MPAD values with fractional parameters deactivated are 2.6588%, 1.6715%, 0.0992%, and 1.6238%, respectively. In contrast, with fractional parameters enabled, the MPAD values improve to 1.4797%, 0.9043%, 0.0898%, and 1.1352%, respectively. These results demonstrate a significant improvement in model accuracy when fractional parameters are incorporated, particularly for the molecular energies considered.

Table 4 summarizes the MPAD values reported for various energy eigenvalue models found in the literature, including the IGPT potential, improved Tietz (ITI) potential, Morse (MOR) potential, modified hyperbolic-type (MHT) potential, improved Scarf (ISC) potential, and improved q-deformed Scarf (IQSC) potential (Yanar et al., 2020; Eyube et al., 2022, Eyube et al., 2021). This table illustrates that incorporating fractional parameters into the equations describing the energy levels of diatomic molecules results in more accurate predictions of energy eigenvalues.

**Table 4: Benchmarking of MPAD values (%) for energy eigenvalues of diatomic molecules**

| Energy model | MPAD with fractional parameters | | | |
|---|---|---|---|---|
| | $Br_2$ ($X\ ^1\sum_g^+$) | $Cl_2$ ($X\ ^1\sum_g^+$) | CO ($X\ ^1\sum^+$) | $Na_2$ ($X\ ^1\sum_g^+$) |
| IGPT | 1.4797 | 0.9043 | 0.0898 | 1.1352 |
| **Energy model** | **MPAD without fractional parameters** | | | |
| | $Br_2$ ($X\ ^1\sum_g^+$) | $Cl_2$ ($X\ ^1\sum_g^+$) | CO ($X\ ^1\sum^+$) | $Na_2$ ($X\ ^1\sum_g^+$) |
| IGPT | 2.6588 | 1.6715 | [e]0.0992, [e]0.0991 | 1.6238 |
| MHT | … | … | [f]0.1001 | … |
| ISC | … | … | [g]0.0991 | … |
| MOR | … | … | [e]0.0989 | … |
| ITI | … | [h]1.0638 | [e]0.3983 | … |
| IQSC | … | [h]1.6845 | … | … |

e: (Yanar et al., 2020); f:(Eyube et al., 2022); g: (Eyube et al., 2022); h: (Eyube et al., 2021)

The applicability of the molar entropy equation is validated by considering the scenario where fractional parameters are disabled. Under these conditions, Equation (20) is equivalent to Equation (16) from (Eyube et al., 2022), which provides the molar entropy formula for the IGPT potential without fractional parameters. This equivalence confirms that Equation (20) represents a general form of the molar entropy model for the IGPT potential.

A novel aspect of this research is the incorporation of fractional parameters into the molar entropy model. Numerical data for the molar entropy (S and $S_{pQ}$) of $Br_2$ ($X\ ^1\sum_g^+$), $Cl_2$ ($X\ ^1\sum_g^+$), CO ($X\ ^1\sum^+$) and $Na_2$ ($X\ ^1\sum_g^+$) molecules are computed using Equation (20), where S denotes the entropy with fractional parameters disabled. The computations are performed at a pressure of 0.1 MPa and over a temperature range of 300 to 6000 K. These results are compared with experimental data from the National Institute of Standards and Technology (NIST, 2017) database, as summarized in Tables 5 and 6. Figures 1-4 present graphical plots of molar entropy versus temperature for these molecules.

**Table 5: Comparative analysis of molar entropy (in J $mol^{-1}K^{-1}$) relative to experimental NIST data for diatomic molecules: PAD values as a percentage of NIST data**

| [i]$T$ (K) | $Br_2$ ($X\ ^1\sum_g^+$) $p$ = 0.5600, $Q$ = 0.5000 | | | | | [i]$T$ (K) | $Cl_2$ ($X\ ^1\sum_g^+$) $p$ = 0.5200, $Q$ = 0.5000 | | | | |
|---|---|---|---|---|---|---|---|---|---|---|---|
| | S | $S_{pQ}$ | [i]$S_{NIST}$ | $PAD_1$ | $PAD_2$ | | S | $S_{pQ}$ | [i]$S_{NIST}$ | $PAD_1$ | $PAD_2$ |
| 300 | 245.982 | 246.287 | 245.617 | 0.1484 | 0.2726 | 300 | 223.135 | 223.667 | 223.289 | 0.0687 | 0.1694 |
| 350 | 251.543 | 251.859 | 251.207 | 0.1337 | 0.2597 | 350 | 228.524 | 229.088 | 228.586 | 0.0270 | 0.2198 |
| 400 | 256.394 | 256.719 | 256.093 | 0.1174 | 0.2446 | 400 | 233.237 | 233.827 | 233.263 | 0.0111 | 0.2419 |
| 450 | 260.696 | 261.029 | 260.431 | 0.1019 | 0.2296 | 450 | 237.427 | 238.039 | 237.446 | 0.0081 | 0.2496 |
| 500 | 264.562 | 264.901 | 264.329 | 0.0883 | 0.2163 | 500 | 241.199 | 241.829 | 241.228 | 0.0119 | 0.2493 |
| … | … | … | … | … | … | … | … | … | … | … | … |
| 1600 | 308.111 | 308.480 | 308.169 | 0.0190 | 0.1009 | 1600 | 284.078 | 284.825 | 284.504 | 0.1498 | 0.1130 |
| 1700 | 310.424 | 310.794 | 310.497 | 0.0234 | 0.0957 | 1700 | 286.364 | 287.114 | 286.813 | 0.1566 | 0.1050 |
| 1800 | 312.612 | 312.982 | 312.700 | 0.0283 | 0.0902 | 1800 | 288.524 | 289.277 | 288.995 | 0.1630 | 0.0975 |
| 1900 | 314.686 | 315.057 | 314.792 | 0.0336 | 0.0842 | 1900 | 290.572 | 291.326 | 291.065 | 0.1695 | 0.0898 |
| … | … | … | … | … | … | … | … | … | … | … | … |
| 2100 | 318.543 | 318.915 | 318.690 | 0.0460 | 0.0706 | 2100 | 294.374 | 295.132 | 294.911 | 0.1821 | 0.0750 |
| 2200 | 320.345 | 320.716 | 320.515 | 0.0532 | 0.0628 | 2200 | 296.147 | 296.907 | 296.707 | 0.1887 | 0.0673 |
| 2300 | 322.071 | 322.443 | 322.269 | 0.0614 | 0.0541 | 2300 | 297.845 | 298.606 | 298.429 | 0.1956 | 0.0594 |
| 2400 | 323.730 | 324.102 | 323.957 | 0.0702 | 0.0448 | 2400 | 299.475 | 300.237 | 300.084 | 0.2029 | 0.0510 |
| … | … | … | … | … | … | … | … | … | … | … | … |
| 5600 | 357.291 | 357.665 | 358.419 | 0.3147 | 0.2104 | 5600 | 332.877 | 333.649 | 334.258 | 0.4132 | 0.1821 |
| 5700 | 357.970 | 358.344 | 359.098 | 0.3140 | 0.2099 | 5700 | 333.582 | 334.354 | 334.941 | 0.4059 | 0.1753 |
| 5800 | 358.636 | 359.009 | 359.761 | 0.3128 | 0.2089 | 5800 | 334.273 | 335.045 | 335.608 | 0.3979 | 0.1677 |
| 5900 | 359.287 | 359.661 | 360.410 | 0.3116 | 0.2079 | 5900 | 334.951 | 335.723 | 336.257 | 0.3884 | 0.1587 |
| 6000 | 359.925 | 360.299 | 361.044 | 0.3100 | 0.2065 | 6000 | 335.616 | 336.389 | 336.891 | 0.3783 | 0.1490 |
| MPAD (%) | | | | 0.1652 | 0.1381 | MPAD (%) | | | | 0.2604 | 0.1360 |

i: (NIST, 2017)

**Table 6: Comparative analysis of molar entropy (in J mol$^{-1}$K$^{-1}$) relative to experimental NIST data for diatomic molecules: PAD values as a percentage of NIST data**

| $^{i}T$ (K) | CO ($X\,^1\Sigma^+$) $p$ = 0.5000, $Q$ = 0.4300 | | | | | $^{i}T$ (K) | $Na_2$ ($X\,^1\Sigma_g^+$) $p$ = 0.5030, $Q$ = 0.4300 | | | | |
|---|---|---|---|---|---|---|---|---|---|---|---|
| | **S** | **$S_{pQ}$** | **$^{i}S_{NIST}$** | **$PAD_1$** | **$PAD_2$** | | **S** | **$S_{pQ}$** | **$^{i}S_{NIST}$** | **$PAD_1$** | **$PAD_2$** |
| 300 | 194.839 | 194.888 | 197.833 | 1.5133 | 1.4886 | 300 | 230.458 | 230.542 | 230.476 | 0.0076 | 0.0286 |
| 400 | 204.008 | 204.069 | 206.238 | 1.0812 | 1.0519 | 350 | 236.195 | 236.280 | 236.286 | 0.0384 | 0.0025 |
| 500 | 211.243 | 211.313 | 212.831 | 0.7462 | 0.7131 | 400 | 241.189 | 241.275 | 241.346 | 0.0651 | 0.0295 |
| 600 | 217.240 | 217.319 | 218.319 | 0.4940 | 0.4579 | 450 | 245.612 | 245.699 | 245.830 | 0.0888 | 0.0535 |
| 700 | 222.375 | 222.461 | 223.066 | 0.3099 | 0.2713 | 500 | 249.583 | 249.671 | 249.859 | 0.1103 | 0.0754 |
| … | … | … | … | … | … | … | … | … | … | … | … |
| 1800 | 255.107 | 255.236 | 254.912 | 0.0764 | 0.1270 | 1600 | 294.941 | 295.031 | 294.755 | 0.0631 | 0.0936 |
| 1900 | 257.042 | 257.173 | 256.859 | 0.0714 | 0.1223 | 1700 | 297.356 | 297.446 | 296.895 | 0.1554 | 0.1857 |
| 2000 | 258.884 | 259.017 | 258.714 | 0.0657 | 0.1170 | 1800 | 299.621 | 299.711 | 298.867 | 0.2522 | 0.2823 |
| 2100 | 260.640 | 260.775 | 260.486 | 0.0592 | 0.1108 | 1900 | 301.748 | 301.838 | 300.692 | 0.3511 | 0.3810 |
| … | … | … | … | … | … | … | … | … | … | … | … |
| 2300 | 263.927 | 264.065 | 263.808 | 0.0452 | 0.0972 | 2100 | 305.636 | 305.726 | 303.976 | 0.5461 | 0.5757 |
| 2400 | 265.470 | 265.609 | 265.369 | 0.0381 | 0.0903 | 2200 | 307.418 | 307.508 | 305.468 | 0.6383 | 0.6678 |
| 2500 | 266.953 | 267.093 | 266.871 | 0.0307 | 0.0831 | 2300 | 309.104 | 309.194 | 306.881 | 0.7243 | 0.7536 |
| 2600 | 268.380 | 268.521 | 268.318 | 0.0232 | 0.0757 | 2400 | 310.702 | 310.792 | 308.227 | 0.8029 | 0.8321 |
| … | … | … | … | … | … | … | … | … | … | … | … |
| 5600 | 296.747 | 296.903 | 297.184 | 0.1471 | 0.0945 | 5600 | 339.355 | 339.445 | 344.731 | 1.5596 | 1.5335 |
| 5700 | 297.410 | 297.566 | 297.862 | 0.1518 | 0.0993 | 5700 | 339.905 | 339.995 | 345.655 | 1.6635 | 1.6375 |
| 5800 | 298.062 | 298.218 | 298.528 | 0.1562 | 0.1037 | 5800 | 340.445 | 340.534 | 346.554 | 1.7629 | 1.7370 |
| 5900 | 298.703 | 298.860 | 299.184 | 0.1608 | 0.1084 | 5900 | 340.974 | 341.064 | 347.428 | 1.8577 | 1.8319 |
| 6000 | 299.333 | 299.490 | 299.829 | 0.1653 | 0.1129 | 6000 | 341.493 | 341.583 | 348.275 | 1.9473 | 1.9215 |
| MPAD (%) | | | | 0.1413 | 0.1322 | MPAD (%) | | | | 0.6449 | 0.6437 |

i: (NIST, 2017)

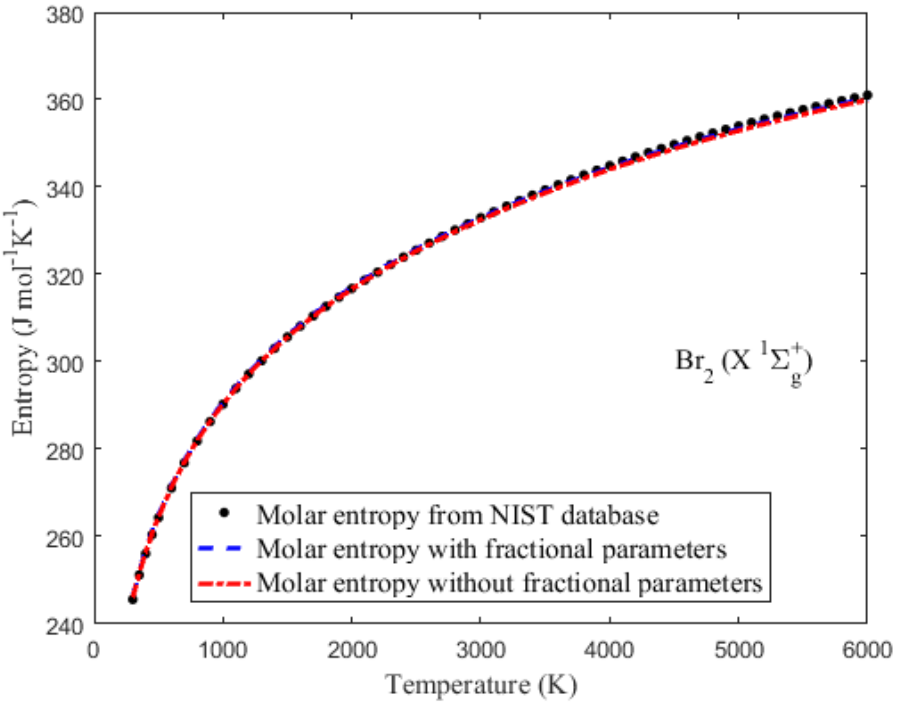


Figure 1: Plot of molar entropy versus temperature for the ground state $Br_2$ dimer

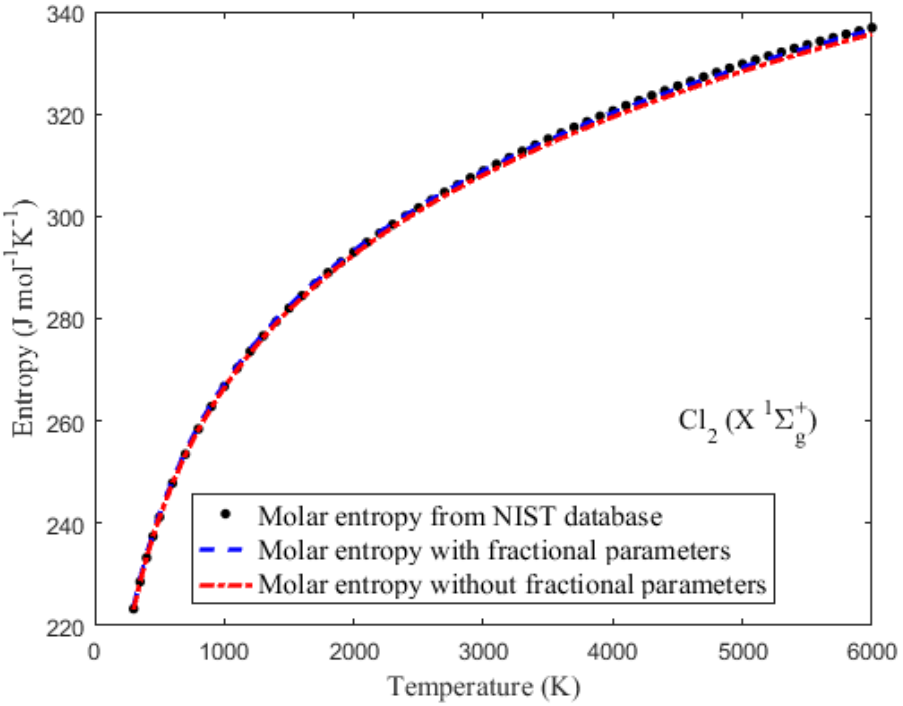


Figure 2: Plot of Molar Entropy Versus Temperature for The Ground State $Cl_2$ Dimer

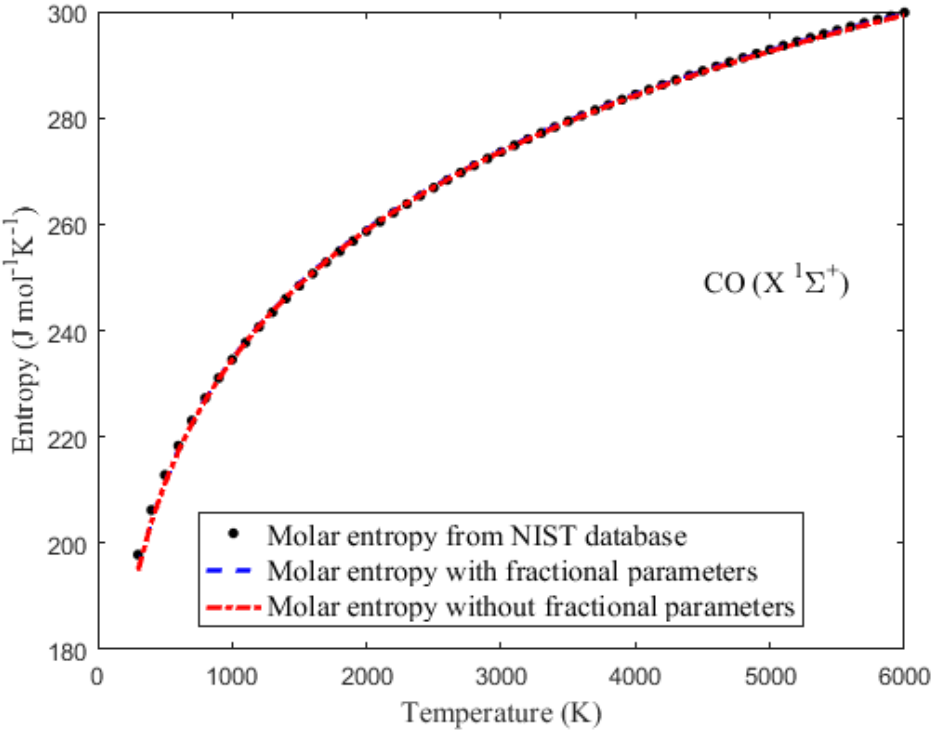


Figure 3: Plot of Molar Entropy Versus Temperature for The Ground State CO Molecule

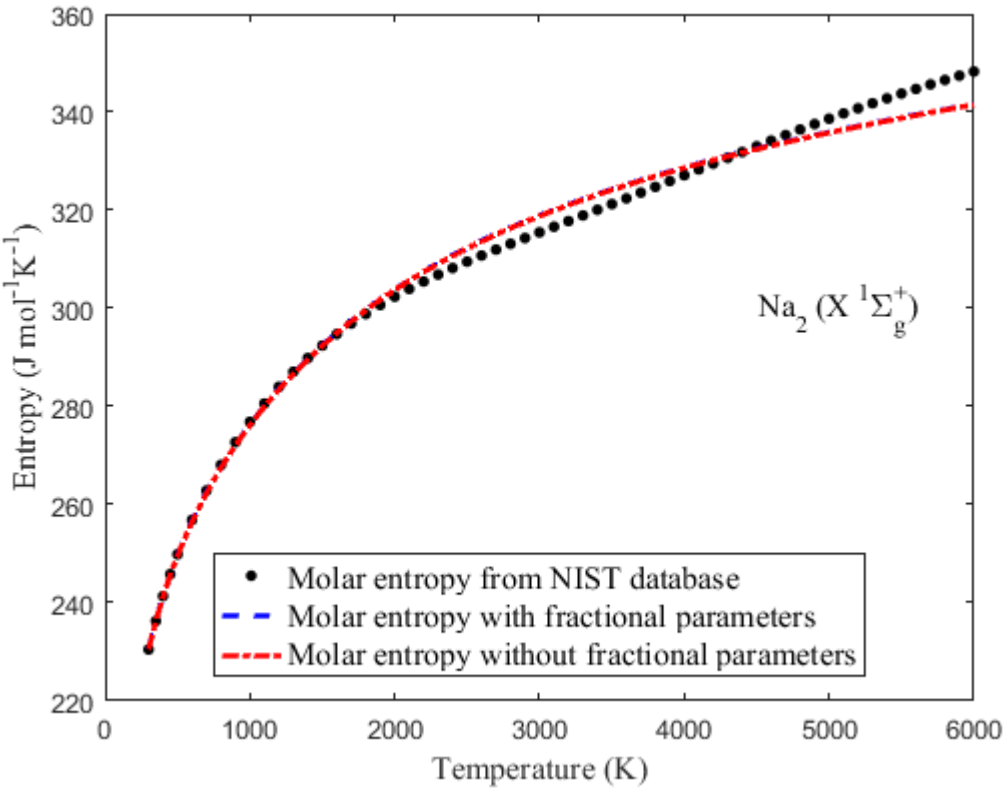


Figure 4: Plot of Molar Entropy Versus Temperature for The Ground State $Na_2$ Dimer

The close agreement between the calculated values and the NIST data confirms the accuracy and applicability of the molar entropy expression. Notably, incorporating fractional parameters enhances the precision of predictions. Analysis of PAD and MPAD values, detailed in Tables 5 and 6, shows that the MPAD values obtained with fractional parameters enabled yield the most accurate molar entropy predictions.

This research introduces a significant advancement by incorporating fractional parameters, improving upon previous models. For instance, Jia et al. (2018) utilizes the improved Tietz (ITI) potential for analyzing thermal properties, while Jia et al. (2019) employed the modified Rosen-Morse (MRM) potential. The findings in Table 7 demonstrate that the IGPT model with activated fractional parameters provides superior MPAD values compared to these existing models, highlighting the importance of fractional parameters in achieving more accurate entropy predictions.

**Table 7: Benchmarking of MPAD values (%) for molar entropy of diatomic molecules**

| **Entropy model** | **MPAD with fractional parameters** | | | |
|---|---|---|---|---|
| | **$Br_2$ ($X\ ^1\Sigma_g^+$)** | **$Cl_2$ ($X\ ^1\Sigma_g^+$)** | **CO ($X\ ^1\Sigma^+$)** | **$Na_2$ ($X\ ^1\Sigma_g^+$)** |
| IGPT | 0.1381 | 0.1360 | 0.1322 | 0.6437 |
| | **MPAD without fractional parameters** | | | |
| **Entropy model** | **$Br_2$ ($X\ ^1\Sigma_g^+$)** | **$Cl_2$ ($X\ ^1\Sigma_g^+$)** | **CO ($X\ ^1\Sigma^+$)** | **$Na_2$ ($X\ ^1\Sigma_g^+$)** |
| IGPT | 0.1652 | 0.2604 | 0.1413 | 0.6449 |
| ITI | 0.5912 | 0.6364 | 0.1425 | 1.2507 |
| MRM | 0.5717 | 0.7148 | 0.5355 | 0.7424 |

## CONCLUSION

In this study, the radial Schrödinger equation is solved using the IGPT potential. The generalized fractional Nikiforov-Uvarov (GFNU) technique is employed to derive explicit equation for pure vibrational energy eigenvalues. By introducing fractional parameters in addition to standard molecular constants, this approach significantly enhances the accuracy of the energy eigenvalues for diatomic molecules. The derived expression for eigen energies is used to construct the internal partition function, which facilitates the calculation of the molar entropy of the system. This methodology is applied to several diatomic molecules, including $Br_2$ ($X\ ^1\Sigma_g^+$), $Cl_2$ ($X\ ^1\Sigma_g^+$), CO ($X\ ^1\Sigma^+$), and

$Na_2$ ($X\ ^1\sum_g^+$). To assess the accuracy of the energy model, the MPAD of the predicted data relative to experimental data is computed. The MPAD values for these molecules are 1.4797%, 0.9043%, 0.0898%, and 1.1352% compared to the Rydberg-Klein-Rees data. For fractional molar entropy, the MPAD values are 0.1381%, 0.1360%, 0.1322%, and 0.6437% relative to the NIST data. The results demonstrate that incorporating fractional parameters into the model equations significantly improves accuracy, as indicated by the lower MPAD values compared to conventional models. This improvement is consistent with existing literature and confirms the dependability of the refined models. The improved accuracy of vibrational energy eigenvalues and molar entropy has prospective applications in several areas, including spectroscopy and molecular detection, chemical kinetics and reaction dynamics, computational chemistry and molecular modeling, and thermodynamics and statistical mechanics.

**REFERENCES**

Abu-Shady, M., and Khokha, E.M. (2023). A Precise Estimation for Vibrational Energies of Diatomic Molecules Using the Improved Rosen-Morse Potential. *Sci. Rep*. 13, 11578. https://doi.org/10.1038/s41598-023-37888-2

Abu-Shady, M., and Fath-Allah, H.M. (2023). The Parametric Generalized Fractional Nikiforov-Uvarov Method and Its Applications. *East Eur. J. Phys*. 3, 248. https://doi.org/10.26565/2312-4334-2023-3-22

Abu-Shady, M., Khokha, E.M., and Abdel-Karim, T.A. (2022) The Generalized Fractional NU Method For the diatomic molecules in the Deng-Fan model. *Eur. Phys. J. D*. 76, 159. https://doi.org/10.1140/epjd/s10053-022-00480-w

Abu-Shady, M., and Khokha, E.M. (2022). On the Prediction of Fractional Vibrational Energies for Diatomic Molecules with the Improved Tietz Potential. *Mol. Phys.* 120, e2140720. https://doi.org/10.1080/00268976.2022.2140720

Ahmed, A.D., Eyube, E.S., Omugbe, E., Onate, C.A., and Timtere, P. (2023). Bound-State Energy Spectrum and Thermochemical Functions of The Deformed Schiöberg Oscillator. *Sci. Rep*. 13, 20386. https://doi.org/10.1038/s41598-023-47235-0

Coxon, J. A. (1980). Revised Molecular Constants, RKR Potential, and Long-Range Analysis for the $B^3\Pi(0_u^+)$ State of $Cl_2$, and Rotationally Dependent Franck-Condon Factors for $Cl_2$ ($BX^1\Sigma_g^+$). *J. Mol. Spectrosc*. 82, 264. https://doi.org/10.1016/0022-2852(80)90116-2

Eyube, E.S., Notani, P.P., Nyam, G.G., Jabil, Y.Y., and Izam, M.M. (2023). Pure Vibrational State Energies and Statistical-Mechanical Models for the Reparameterized Scarf Potential. *Front. Phys*. 11, 978347. https://doi.org/10.3389/fphy.2023.978347

Eyube, E.S., Notani, P.P., and Dikko, A.B. (2022). Modeling of Diatomic Molecules with Modified Hyperbolical-Type Potential. *Eur. Phys. J. Plus*, 137, 329. https://doi.org/10.1140/epjp/s13360-022-02526-9

Eyube, E.S., Notani, P.P., and Izam, M.M. (2022). Potential Parameters and Eigenspectral of Improved Scarf II Potential Energy Function for Diatomic Molecules. *Mol. Phys*. 120, e1979265. https://doi.org/10.1080/00268976.2021.1979265

Eyube, E.S., Bitrus, B.M., Samaila, H., and Notani, P.P. (2022). Model Entropy Equation for Gaseous Substances. *Int. J. Thermophys*. 43, 55. https://doi.org/10.1007/s10765-022-02980-8

Eyube, E.S., Notani, P.P., Samaila, H. (2022). Analytical Prediction of Enthalpy and Gibbs Free Energy of Gaseous Molecules. *Chem. Thermodyn. Thermal Anal*. 6, 100060. https://doi.org/10.1016/j.ctta.2022.100060

Eyube, E.S., Onate, C.A., Omugbe, E., and Nwabueze, C.M. (2022). Theoretical Prediction of Gibbs Free Energy and Specific Heat Capacity of Gaseous Molecules. *Chem. Phys*. 560, 111572. https://doi.org/10.1016/j.chemphys.2022.111572

Eyube, E.S., Nyam, G.G., and Notani, P.P. (2021). Improved q-deformed Scarf II Potential. *Phys. Scr*. 96, 125017 https://doi.org/10.1088/1402-4896/ac2eff

Focsa, C., Li, H., and Bernath, P. F. (2000). Characterization of the Ground State of $Br_2$ by Laser-Induced Fluorescence Fourier Transform Spectroscopy of the $B^3\Pi_{0+u}$-$X^1\Sigma_g^+$ System. *J. Mol. Spectrosc*. 200, 104. https://doi.org/10.1006/jmsp.1999.8039

Garbett, N. C., and Chaires, J. B. (2012). Thermodynamic studies for drug design and screening. *Expert Opin. Drug Discov*. 7, 299. https://doi.org/10.1517/17460441.2012.666235

Hajigeorgiou, P. G. (2010). An Extended Lennard-Jones Potential Energy Function for Diatomic Molecules: Application to Ground Electronic States. *J. Mol.*

*Spectrosc*. 263, 101. https://doi.org/10.1016/j.jms.2010.07.003

Jia, C. S., Zhang, L. H., Peng, X. L., Luo, J. X., Zhao, Y. L., Liu, J. Y., Guoa, J.J., Dong, L., and Tang, L.D. (2019). Prediction of Entropy and Gibbs Free Energy for Nitrogen. *Chem. Eng. Sci*. 202, 70. https://doi.org/10.1016/j.ces.2019.03.033

Jia, C. S., Wang, C. W., Zhang, L. H., Peng, X. L., Tang, H. M., Liu, J. Y., Xiong, Y., and Zeng, R. (2018). Predictions of Entropy for Diatomic Molecules and Gaseous Substances. *Chem. Phys. Lett*. 692, 57. https://doi.org/10.1016/j.cplett.2017.12.013

Kirschner, S. M., and Watson, J. K. G. (1974). Second-Order Semiclassical Calculations for Diatomic Molecules. *J. Mol. Spectrosc*. 51, 321. https://doi.org/10.1016/0022-2852(74)90060-5

Kusch, P., and Hessel, M. M. (1978). An Analysis of the B $^1\Pi_u$–X $^1\sum_g^+$ Band System of $Na_2$. *J. Chem. Phys*. 68 (1978) 2591. http://dx.doi.org/10.1063/1.436117

National Institute of Standards and Technology (NIST), NIST Chemistry WebBook, NIST Standard Reference Database Number 69 (2017). https://doi.org/10.18434/T42S31

Onate, C.A., Okon, I.B., Omugbe, E., Eyube, E.S., Al-Asbahi, B.A., Kumar, Y.A., Emeje, K.O., Aghemenloh, E., Obasuyi, A.R., Obaje, V.O., and Etchie, T.O. (2924). *Chem. Phys*. 582, 112294. https://doi.org/10.1016/j.chemphys.2024.112294

Popovic, M., and Minceva, M. (2021). Standard Thermodynamic Properties, Biosynthesis Rates, and the Driving Force of Growth of Five Agricultural Plants. *Front. Plant Sci*. 12, 671868. https://doi.org/10.3389/fpls.2021.671868

Shamsabadipour, A., Pourmadadi, M., Davodabadi, F., Rahdar, A., and Ferreira, L.F.R. (2023). Applying Thermodynamics as An Applicable Approach to Cancer Diagnosis, Evaluation, and Therapy: A Review. *J. Drug Deliv. Technol*. 85, 104681. https://doi.org/10.1016/j.jddst.2023.104681

Strekalov M.L. (2024). The Heat Capacity of Triatomic Gases: An Analytical Approach. *Int. J. Thermophys*. 45, 25. https://doi.org/10.1007/s10765-023-03315-x

Williams, I., Turci, F., Hallett, J. E., Crowther, P., Cammarota, C., Biroli, G., and Royall, C. P. (2018). Experimental Determination of Configurational Entropy in A Two-Dimensional Liquid Under Random Pinning. *J. Phys. Condens. Matter* 30, 094003. https://doi.org/10.1088/1361-648X/aaa869

Yanar, H., Taş, A., Salti, M., and Aydogdu, O. (2020). Ro-Vibrational Energies of CO Molecule via Improved Generalized Pöschl–Teller Potential and Pekeris-Type Approximation. *Eur. Phys. J. Plus* 135, 292. https://doi.org/10.1140/epjp/s13360-020-00297-9